A general method to determine optimal thermal cycles based on solid-state sintering fundamentals

Antonio Barba | Carolina Clausell

Department of Chemical Engineering, Instituto Universitario de Tecnología Cerámica

Universitat Jaume I, 12006-Castellón, Spain

Abstract

Most technical ceramics require processing up to and including final-stage sintering to obtain a high-density bulk while inhibiting grain growth as dominant sintering process as far as possible. The literature typically highlights the qualitative interdependence of the sintering variables and microstructural parameters, focusing on very simple particulate systems. However, a quantitative method to achieve optimum sintering of actual polycrystalline solids is still lacking.

This paper puts forward such a method, which has been satisfactorily tested by the authors. The method consists of a mathematical model, based on the physical phenomena that take place during solid-state sintering. The method leads to two differential equations: a densification rate and a pore-dragged normal grain growth rate equation during final-stage sintering, which mainly depend on sintering temperature and shaping conditions. Simultaneous numerical integration of these two rate equations allows design of an optimal thermal cycle (enhancing densification and controlling grain growth) to obtain the targeted sintered polycrystalline microstructure. Application of this method yields staggered thermal cycles, in addition to the number of steps, as well as the sintering temperature and dwell time in each step.

KEYWORDS

Solid-state sintering, densification rate and grain growth rate, thermal cycle

1. INTRODUCTION

In the manufacture of technical ceramics, body chemical composition and microstructure are specified to optimize the mechanical, electric, dielectric, optical, thermal, magnetic or other physical property of the resulting product for a particular application. The optimum properties are defined by the microstructure. This requires thorough microstructural control, including relative density (total porosity) and grain and pore size distributions, particularly average grain and pore sizes. Optimal microstructure requires defining and controlling the main parameters of the manufacturing process. Sintering is a key step in manufacturing ceramic bodies that exhibit a targeted final microstructure, although this also depends on green body microstructure (related to shaping conditions).

Many studies were undertaken in the 20th century to better understand the mechanisms involved in solid-state sintering. Good summaries may be found in the literature[1–3]. Many of the theoretical models and discussions have been based on hard hypotheses, designed to simplify the physical process (e.g. by drastically simplifying pore shape and size), and they have usually been applied to systems of few particles and not to consolidated solids. These studies have helped understand why and how sintering takes place, evidencing the interdependence of the sintering variables and the microstructural parameters, generally by deriving theoretical equations that have often been used in numerical simulation or modelling[4–11] of unreal solids[1–3]. However, these equations only allow qualitative conclusions to be drawn.

A method of applying the existing models to real solids, enabling determination of sintering temperature and time on an industrial scale to obtain a targeted microstructure

(usually characterized by relative density and average grain size), is thus still lacking. Though this may be deemed a major research aim, most current work focuses on the micro- or nano-properties[12–15] of very simple particulate systems (not of bulk solids), whereas the main difficulty is holding the intrinsic properties of these simple particulate systems during the sintering of bulk polycrystalline solids in industrial practice.

The present study was therefore undertaken to develop a method, which has been satisfactorily tested by the authors[16–18], to quantitatively relate the final sintered microstructure of a bulk polycrystalline ceramic to the customary industrial control parameters set in the solid-state sintering stage of the thermal cycle used. That is, the proposed method establishes the mathematical correlations between the vertices of the materials science triangle (processing–properties–microstructure) in order to design the final microstructure and thus obtain the targeted product properties.

To develop this method, the theoretical basis of solid-state sintering was examined first, to better understand the force that drives sintering, the mass transfer mechanisms involved, the rate at which mass transfer occurs in both densification and grain growth, and how these last two processes interact. A brief description of this preliminary study, which sets out the fundamentals of the proposed method, follows.

Sintering thermodynamics and mechanics

Sintering involves two simultaneous processes, which are parallel and competitive: densification and grain growth, which bring the final density of the ceramic body close to its theoretical density.

According to thermodynamics, sintering is driven by the decrease in internal energy at the surface ($\gamma \cdot A$), which can be modified by replacing gas–solid surface energy (γ_{s-g}) with solid–solid surface energy (γ_{s-s}) and/or surface area (A). The potential combinations

explain the possible processes that can develop in polycrystalline solid materials: coarsening, densification, and grain growth (see Figure 1)[19–24].

Mass transfer proceeds from convex to concave grain surfaces to achieve thermodynamic equilibrium[3]. This mass gradient is evidenced by a total pressure gradient (Young–Laplace law), atoms or vacancies gradient (Gibbs–Thompson–Freundlich equation), and partial pressure gradient (Kelvin equation), mass transfer taking place by diffusion according to the Nernst–Einstein equation and Fick's law[1].

Similar to thermodynamic equilibrium, a particulate solid system must achieve an equilibrium of mechanical forces, so that the sine, dihedral angle, and wetting angle equations must be met (the last equation being just for liquid-phase sintering). If all these equations are met, assuming that all grains have the same size, the grain geometry that yields maximum packing is the tetrakaidecahedron (a truncated octahedron). This is the most commonly used geometry in the sintering models reported in the literature[3].

Since thermodynamics allows sintering to take place, the key issue is to determine both the densification rate and the grain growth rate, in order to establish the duration and temperature of the sintering stage and to ascertain microstructural development.

Densification and grain growth

The densification process has traditionally been divided into three stages (depending on the relative density of the body), while the grain growth process is usually divided into normal and abnormal grain growth. Densification and grain growth have typically been studied independently, it being assumed that densification takes place without grain growth and that grain growth develops in 100% densified bodies. Densification and grain

growth are therefore assumed to be consecutive and uncompetitive processes, whereas in fact they occur simultaneously and competitively.

The individual kinetic study of these processes allows their physical development to be understood, the variables involved to be determined, and the influence of these variables on kinetics to be ascertained. However, the applicability of the assumptions made in the kinetic models will depend on how far removed such assumptions are from the actual system.

Densification of pore solids without grain growth

Stages I, II, and III of the densification process were widely studied in the 20th century. The simplest theoretical model put forward for initial-stage sintering (stage I) has been the two-particle model. Similarly, intermediate- and final-stage sintering (stages II and III) has generally been described using the tetrakaidecahedron model, this being the geometry that provides mechanical equilibrium. In the intermediate stage, the pores are described as cylinder-shaped, located along tetrakaidecahedron grain edges. In the final stage, the pores are assumed to be sphere-shaped, located at the corners of the tetrakaidecahedron grains[1–3,25].

The physical models used in these three sintering stages are based on the same mass transfer mechanisms: (i) Mass transfer from solid–gas surface to solid–gas surface, which leads to coarsening but not densification. The mass transfer mechanisms in this case are evaporation–condensation and diffusion (through the gas phase, and surface or bulk (or lattice) diffusion). (ii) Mass transfer from solid–solid surface (grain boundary) to the solid–gas surface, this being the only mechanism enabling body densification. The mass transport mechanism in this case is diffusion, through the grain boundary and/or bulk (or lattice) diffusion.

The main mass transfer mechanism is diffusion[6], which follows Fick's law. The kinetics equation can be obtained from the mass balance, and its integration form provides a relationship between relative density and time[3].

In the mass transport process, the rate of atom movement depends on the forces acting on the atoms. As noted above, the difference in particle curvature leads to a concentration difference, which generates atom transfer. This concentration difference is the movement force, which is related to the atomic rate of the transfer phenomena by a proportional coefficient, atomic mobility (M_a). Einstein thus defined atomic mobility as the quotient of atomic rate and force ($M_a = v_a/F_a$)[26].

Grain growth without densification

Fully dense solids

Most studies have focused on normal grain growth (abnormal grain growth only being of interest when there was a material property that needed a spatial orientation). The understanding of normal grain growth is grounded on the Ostwald ripening effect, which is based on the concentration gradient due to grain curvatures: smaller grains having smaller curvature radii cause mass transfer to bigger grains. Mass transfer could be controlled by diffusion or interfacial reaction. Subsequent authors proposed a kinetic equation to model the Ostwald ripening effect. Their model, known as the LSW model[3], though quite simple, satisfactorily describes most experimental observations in precipitate growth.

The first model used for understanding grain growth in polycrystalline solid materials was proposed by Burke and Turnbull[3]. In this model, grain growth takes place by atomic mass transfer through the grain boundary, caused by a chemical potential gradient due, again, to surface curvature. Einstein's definition of atomic mobility was extended to

the concept of grain boundary mobility, defined as the quotient of grain boundary rate and the force causing this movement ($M_{gb} = v_{gb}/F_{gb}$). Applying mass balance to the grain boundary, together with Fick's law, these authors put forward a parabolic law relating grain size to sintering time (similar to Ostwald ripening controlled by interfacial reaction). In practice, however, a power law must be used instead of the parabolic law in the theoretical model.

Nevertheless, the most interesting feature of the Burke and Turnbull model was that it provided an understanding of the different mechanisms that controlled grain boundary mobility, in order to decrease or even inhibit the grain growth process. The model shows that grain boundary mobility can basically be changed either by a physical procedure (adding smaller secondary particles) or by a chemical procedure (adding chemical dopants).

When secondary particles are dispersed in a polycrystalline solid, they hinder or even inhibit grain growth. This is usually known as the pinning effect and was modelled by Zener [1–3] assuming that secondary particles exert a physical friction force (drag force), which decreases grain boundary mobility. Considering this drag force in the Burke and Turnbull model enables the new grain growth rate to be obtained. It is also enables maximum grain size to be determined when grain growth halts because of the drag force. Although the Zener model has been refined by various researchers[1–3], it remains essentially valid and allows grain size to be controlled.

When a small quantity of chemical dopant (solute) is added to a (host) polycrystalline solid, it dissolves in the grain boundary, forming a solid solution with a different chemical composition to that of the host. Dopants modify the chemical composition of the grain boundary, thus causing dopant and host atom diffusivities through the grain boundary to change. When the grain boundary moves, the solute concentration profile in the grain

boundary becomes asymmetrical, generating a *frictional* or *drag force* of a chemical nature, decreasing the grain boundary migration rate. The driving force acting on the grain boundary now depends not only on the host atom concentration gradient through the grain boundary but also on the solute atom concentration gradient. Cahn, Lucke, and Stuwe applied mass balance and Fick's law to mass transfer through the grain boundary of host and solute atoms[1–3]. They modelled the system, concluding that the inverse of grain boundary mobility ($1/M_{gb}$) was the sum of the inverses of original grain boundary mobility (without dopants) ($1/M_0$), which was only due to the host atom concentration gradient because of surface curvature, plus grain boundary mobility, due only to the solute atom concentration gradient ($1/M_s$).

Pore solids

The grain growth process in solid-state sintering actually takes place in a porous matrix. In most cases, sintering is intended to produce fully dense or quasi-fully dense bodies, in order to obtain good physical properties, therefore requiring sintering to start from high-dense green bodies. This makes it particularly interesting to understand grain behaviour in the presence of pores in final-stage sintering. Quantitative approaches have been based on an ideal structure containing spherical pores on the grain boundaries, the pores being classified as either mobile or immobile.

Immobile pores are described using the Zener model for secondary particles: the pores exert a pinning effect on the grain boundary, inhibiting boundary migration, or are trapped inside the grains. However, there is no convincing evidence regarding pore immobility during sintering of polycrystalline materials. In contrast, much evidence is available on pore mobility[27–30].

The Brook model allows theoretical analysis of grain growth in a porous matrix[27]. Mathematical simulation enables very useful, albeit only qualitative, conclusions to be obtained from a conceptual point of view.

Mobile pores move together with the grain boundary and, in analogy to atomic mobility and grain boundary mobility in fully dense solids, pore mobility is defined as the quotient of the pore rate and the force causing this movement ($M_p = v_p/F_p$)[1–3]. The moving grain boundary, caused by boundary curvature, exerts a force on the pore, changing pore form. The difference in curvature produces an atomic concentration gradient that gives rise to mass transfer (by evaporation/condensation, gas, surface and/or bulk diffusion) from the leading surface to the trailing surface of the pore. Pore mobility is related to a power law of the inverse of pore radius, and the value of the exponent depends on the mass transfer mechanism. Pore mobility allows the pore–grain boundary interaction and its influence on grain growth kinetics to be analysed.

Two situations are reported in the literature[6,7,27,31]: (i) The pore breaks away from the grain boundary. This occurs when a pore moves more slowly than the grain boundary and therefore becomes trapped in the grain (blue area in Figure 2). (ii) The pore moves together with the grain boundary. This occurs when both move at the same speed (two reddish areas in Figure 2). These two areas are delimited by the so-called separation curve.

If pores move together with the grain boundary (entire reddish area in Figure 2), there are also two scenarios: pore control and grain boundary control. Pore control takes place when pore mobility is lower than the product of grain boundary mobility and number of pores per grain ($M_p < M_{gb} \cdot N$), which usually occurs for big pores having slow mobility. Otherwise, grain boundary control takes place when pore mobility is higher than the product of grain boundary mobility and number of pores per grain ($M_p > M_{gb} \cdot N$), which

generally occurs with small pores that do not exert a significant drag force on the grain boundary. These two scenarios are delimited by the so-called isomobility line.

In the above two situations and scenarios, grain size again follows a power law with time. The aim is to work as far as possible away from the separation area: however, the real challenge is to know how to achieve this aim when sintering an actual bulk material.

Microstructural development: sintering (simultaneous densification and grain growth)

As noted above, sintering involves two simultaneous competitive processes: densification and grain growth. Each process is extremely complex and influences the other. In fact, to perform a theoretical analysis by coupling the two processes is very difficult. Moreover, both processes take place in a porous matrix.

Few approaches have developed quantitative relationships between density, grain size, and sintering temperature and time owing to the difficulties posed, which include the large number of variables that need to be studied. Most available theoretical models are non-predictive models, which only allow *a priori* general guidelines and an *a posteriori* qualitative explanation of the resulting final microstructure to be obtained. Studies reported in the literature[28–30,32–34] are based on an ideal microstructure at final-stage sintering start: the grains are tetrakaidekahedron-shaped, the pores are virtually spherical and located at the grain edges, the number of pores per grain is constant, there is no pore–grain boundary separation and, finally, the densification and grain growth mechanisms do not change during sintering.

The studies mentioned indicate that both sintered body density and grain size depend on the densification rate and the grain growth rate according to the following generalized equations:

$$\frac{1}{\phi(t)} \cdot \frac{d\phi(t)}{dt} = J_{1i} \cdot \frac{[1-\phi(t)]^k}{\phi(t) \cdot G(t)^m} \quad (1)$$

$$\frac{1}{G(t)} \cdot \frac{dG(t)}{dt} = J_{2i} \cdot \frac{1}{[1-\phi(t)]^\ell \cdot G(t)^n} \quad (2)$$

where ϕ is relative density (ratio of density to theoretical density) and G is average grain size.

Equations 1 and 2 apply to the densification and pore-drag normal grain growth rates (pore control or grain boundary control areas in Figure 2) during final-stage sintering. Both equations, relating relative density (ϕ) and average grain size (G) to sintering time, have been put forward in the literature[3,28–30] for determining the microstructural development of sintered polycrystalline specimens. Owing to the difficulty of simultaneously integrating these equations, only qualitative conclusions are usually reported in the literature.

2. THEORETICAL BASIS FOR DEFINING A GENERAL METHOD

A quantitative method for determining sintering temperature and time in real solids on an industrial scale, by applying equations 1 and 2, is still lacking. Such a method needs to allow microstructure development (G and ϕ) with sintering time (t) to be predicted, in order to obtain a targeted final microstructure.

From a process engineering point of view, such a method would be very useful, as technical ceramics require processing up to and including final-stage sintering in order to obtain a high-density body while inhibiting grain growth as far as possible[3]. According to equations 1 and 2 and to the literature, in a non-pressure-assisted sintering process, there are three ways of enhancing a material's densification process: (i) by increasing sintering temperature (implicit in J_{1i} and J_{2i}); (ii) by decreasing the mean particle size of the raw materials, making the raw materials more reactive (initial G); and (iii) by

increasing green density (initial ϕ). However, it is physically impossible to increase the relative density of a specimen without also promoting particle growth[35].

The best approach thus appears to be design of a suitable thermal cycle, particularly as the chemical composition must not be altered.

In this paper, a mathematical solid-state sintering model is therefore proposed, based on the physical phenomena that take place during the sintering stage. The model enables equations 1 and 2 to be solved, yielding:

i) a densification rate and a grain growth rate equation.

ii) design of an optimal thermal cycle to increase the densification rate, while controlling the grain growth rate, in order to obtain a highly densified sintered body with low grain growth (microstructural control).

iii) the material transport-controlling mechanisms in densification and grain growth.

However, in contrast to what is commonly found in the literature[3,15], equations 1 and 2 need to be expressed as follows[5,28–30]:

$$\frac{d\phi}{dt} = J_{1i} \cdot \frac{(1-\phi)^k}{G^m} \quad (3)$$

$$\frac{dG}{dt} = J_{2i} \cdot \frac{1}{(1-\phi)^{\ell} \cdot G^{n-1}} \quad (4)$$

in order to have a system of two differential equations (equations 3 and 4), which can be easily integrated using a numerical method.

In addition, equations 3 and 4 contain non-homogeneous units: the densification rate is in s^{-1} while the grain growth rate is in $\mu m \cdot s^{-1}$. It is therefore convenient to introduce a new variable, dimensionless grain size η, as the quotient of grain size (G) and mean particle

size before sintering start (d_{50}). In accordance with the definition of dimensionless grain size, equations 3 and 4 may then be rewritten as follows:

$$\frac{d\phi}{dt} = K_{1i} \cdot \frac{(1-\phi)^k}{\eta^m} \quad (s^{-1}) \tag{5}$$

$$\frac{d\eta}{dt} = K_{2i} \cdot \frac{1}{(1-\phi)^{\ell} \cdot \eta^{n-1}} \quad (s^{-1}) \tag{6}$$

Equations 5 and 6 can be numerically integrated. They have an independent variable (t) and two time-dependent variables (ϕ and η). As dimensionless grain size affects the denominator of both rates, in real systems, dimensionless grain size will either have the same effect on both rates ($m = n - 1$) or will affect both rates differently ($m \neq n - 1$). Note, however, that relative density appears in the numerator in equation 5 and in the denominator in equation 6 (taking into account that exponents k and ℓ are equal to zero or higher).

The relative influence of relative density and dimensionless grain size on both rates cannot be compared *a priori*, because both variables are interrelated. This has led some authors to draw erroneous conclusions on comparing both rates. Sometimes, however, equations 5 and 6 have been compared, disregarding the fact that such a comparison is only possible if one of the two dependent variables (ϕ or η) is assumed to be constant throughout sintering, which is far removed from what occurs in real sintering[3].

The values of coefficients k and m in equation 5 are related to the mass transfer mechanism (diffusion path) (Table 1). The values of the ℓ and n coefficients in equation 6 are not just related to the mass transfer mechanisms in pore-drag grain growth, but also depend on the conditions of grain boundary migration (pore or grain boundary control) (Table 2).

In the proportionality constants K_{1i} and K_{2i} in equations 5 and 6, '1' refers to the densification process (equation 5) and '2' to the grain growth process (equation 6), while subscript 'i' depends on the material transport mechanisms controlling each of these processes. According to Tables 1 and 2, there are 10 possible combinations of mass transfer mechanisms.

K_{1i} and K_{2i} include the effect of sintering temperature and green microstructure. They are mathematical functions relating to the number of pores per grain (N), the diffusion coefficients for densification (D_d) and grain growth (D_g), solid–gas surface energy (γ_{s-g}), molar volume of the diffusing species (Ω), Boltzmann constant (K), absolute temperature (T), and average particle size (d_{50}), while C_d and C_g are constants relating to the mass transfer-controlling mechanism in densification and grain growth, respectively. K_{1i} and K_{2i} are usually experimentally determined for every sintering system. They are related to sintering temperature through an empirical Arrhenius-type equation as follows:

$$K_{1i} = \frac{C_d \cdot N \cdot D_d \cdot \gamma_{s-g} \cdot \Omega}{k \cdot T \cdot d_{50}^{m}} \approx K_{1i0} \cdot exp\left(\frac{-H}{T}\right) \tag{7}$$

$$K_{2i} = \frac{C_g \cdot N^{\frac{1}{n-1}} \cdot D_g}{d_{50}^{n-1}} \approx K_{2i0} \cdot exp\left(\frac{-L}{T}\right) \tag{8}$$

where the pre-exponential terms (K_{1i0} and K_{2i0}) and the exponential terms (H and L) of equations 7 and 8 are likely to be empirically related to some shaping parameter determining green microstructure, such as the pressing pressure used for shaping the ceramic bodies by uniaxial pressing[17].

Unlike the usual approach[3], the ratio of grain growth rate to densification rate (Γ) needs to be calculated as follows:

$$\Gamma = \frac{\frac{d\phi}{dt}}{\frac{d\eta}{dt}} = \frac{d\phi}{d\eta} = \frac{K_{1i}}{K_{2i}} \cdot \frac{\frac{(1-\phi)^k}{\eta^m}}{\frac{1}{(1-\phi)^{\ell} \cdot \eta^{n-1}}} = \frac{K_{1i}}{K_{2i}} \cdot (1-\phi)^{k+\ell} \cdot \eta^{n-m-1} \tag{9}$$

integration of which yields the following relationship between ϕ and η:

$$(1-\phi_0)^{1-k-\ell} - (1-\phi)^{1-k-\ell} = \frac{K_{1i}}{K_{2i}} \cdot \frac{(1-k-\ell)}{(n-m)} \cdot (\eta^{n-m} - \eta_0^{n-m}) \quad (10)$$

However, equation 10 is not mathematically valid when $m = n$. Instead, integration of equation 9, considering $m = n$, yields the following expression:

$$(1-\phi_0)^{1-k-\ell} - (1-\phi)^{1-k-\ell} = \frac{K_{1i}}{K_{2i}} \cdot (1-k-\ell) \cdot ln\frac{\eta}{\eta_0} \quad (11)$$

The plot of dimensionless grain size versus relative density results in a curve, for a given green microstructure, such as the one shown in Figure 3 (for any k, ℓ, m, and n coefficients).

3. DEVELOPMENT OF A GENERAL METHOD

Figure 4 provides an overview of the general method set out in this paper for simultaneous determination of densification and grain growth in final-stage solid-state sintering, with a view to defining the optimal thermal cycles, as explained below.

3.1. Experimental data needed

The experimental data needed for physical–mathematical modelling to design the thermal cycle are the dimensionless densification (ϕ) and dimensionless grain size (η) of the polycrystalline specimens shaped under different conditions (depending on the green process selected) and sintered at different temperatures (T) and different dwell times (t) (see Figures 5 and 6).

Specimens with the same green microstructure must be sintered at different sintering temperatures (T) and times (t). Generally, relative density (ϕ) is calculated as the quotient of experimental density (ρ), determined by the Archimedes method, and theoretical density (ρ_t). Average grain size (G) is measured from the grain size distribution,

determined by image analysis of the cross-sectional area of the rectangular thermal etched surface of each cylindrical sintered specimen, observed by scanning electron microscopy (SEM).

In overall terms, the following may be inferred from Figure 5 (for a given green microstructure): (i) ϕ increases quickly at short sintering times and slowly at long sintering times, tending to a constant value. This change in tendency is more abrupt at higher sintering temperatures, and smoother at lower ones. (ii) The higher the sintering temperature, the higher the value of ϕ, a shorter sintering time therefore being required to achieve this. (iii) The densification rate increases with sintering temperature, as the tangent to the curve at each point.

In overall terms, the following may be inferred from Figure 6 (for a given green microstructure): (i) η increases with sintering time in a certain sintering temperature range (depending on the nature of the material). Higher sintering temperatures yield huge η values (i.e. abnormal or exaggerated grain growth), which remain practically constant with sintering time. Lower sintering temperatures yield very small η values, which may even be very similar to initial particle size when sintering temperature is particularly low. (ii) In the normal grain growth range, η increases more quickly at shorter sintering times and more slowly at longer ones, tending to a constant value. This change in tendency is more abrupt at higher sintering temperatures, and smoother at lower ones. (iii) The higher the sintering temperature, the higher the value of η, a shorter sintering time therefore being required to achieve this. (iv) The grain growth rate increases with sintering temperature, as the tangent to the curve at each point.

These trends are similar for any green microstructure, whereas ϕ and η change with the selected shaping parameter.

The experimental data need to be analysed, first, by a differential method in order to determine the k, ℓ, m, and n coefficients in equations 5 and 6 and, secondly, by an integration method to determine the densification and grain growth rate equations.

3.2. Determination of coefficients k, ℓ, m, and n and estimation of parameters K_{1i} and K_{2i} in equations 5 and 6 by a differential method

The first step in the differential method is the generation of the $d\phi/dt = f(t)$ and $d\eta/dt = f(t)$ graphical representations, obtained from the $\phi = f(t)$ and $\eta = f(t)$ experimental curves, as the tangent to the curve at each time.

The $d\phi/dt = f(t)$ representation may be linearized by rewriting equation 5 as follows:

$$ln\left(\frac{d\phi}{dt}\right) - k \cdot ln(1-\phi) = ln(K_{1i}) - m \cdot ln(\eta) \quad (12)$$

and plotting the experimental data of $\ln(d\phi/dt) - k \cdot ln(1-\phi)$ versus $ln(\eta)$ (Figure 7), the K_{1i} and m values can be estimated and determined, respectively, for the given pre-set values of k from Table 1. The correct value of k and m will allow the best linear fit of the experimental data to equation 12.

Analogously, the $d\eta/dt = f(t)$ representation may be linearized by rewriting equation 6 as follows:

$$ln\left(\frac{d\eta}{dt}\right) + \ell \cdot ln(1-\phi) = ln(K_{2i}) - (n-1) \cdot \ln(\eta) \quad (13)$$

and plotting the experimental data of $\ln(d\eta/dt) + \ell \cdot ln(1-\phi)$ versus $ln(\eta)$ (Figure 8), the K_{2i} and $(n-1)$ values can be estimated and determined, respectively, for a given pre-set value of ℓ from Table 2. The correct value of ℓ and $(n-1)$ will allow the best linear fit of the experimental data to equation 13.

This analysis method has two main drawbacks: (i) the need to draw the curves of the experimental data $\phi = f(t)$ and $\eta = f(t)$, and (ii) the need to calculate the tangent to the

curve at each experimental point in order to obtain the $d\phi/dt = f(t)$ and $d\eta/dt = f(t)$ representations. Operations (i) and (ii) are critical[36]. Consequently, when sufficient information on the system at issue is available, use of the integration method is more convenient.

The above method applies to the test sintering temperature range and to a given green microstructure and may be repeated for different shaping conditions. The method may be repeated for different green microstructures. It is thus possible to estimate the influence of temperature and green microstructure on parameters K_{1i} and K_{2i}, since coefficients $k, \ell, m,$ and $(n-1)$ remain unchanged.

3.3. Refinement of parameters K_{1i} and K_{2i} in equations 5 and 6 by simultaneous integration of the rate equations

Equations 5 and 6 can be rewritten by replacing coefficients $k, \ell, m,$ and $(n-1)$ with their values, determined either by the above differential method or from the literature. Their simultaneous integration allows determination of parameters K_{1i} and K_{2i}, as well as of the values of ϕ_0 and η_0 (relative density and dimensionless grain size when sintering temperature has been reached, i.e. at zero sintering time). Initial conditions need to be set for the integration method, so that a previously estimated value of K_{1i} and K_{2i} (estimated by the differential method) and of ϕ_0 (green relative density) and $\eta_0 = 1$ is required. Simultaneous integration of equations 5 and 6 also requires use of a numerical mathematical method.

The representation of $ln(K_{1i}) = (1/T)$ and $ln(K_{2i}) = (1/T)$ yields two empirical relationships between parameters K_{1i} and K_{2i} and sintering temperature, where the exponential (H and L) and pre-exponential (K_{1i0} and K_{2i0}) factors of equations 7 and 8 (according to the Arrhenius law) can also be related to the selected shaping parameter

(P), yielding a general empirical equation of parameters K_{1i} and K_{2i} with sintering temperature and green microstructure.

The densification and grain growth rates of the studied polycrystalline material, under a given set of conditions, can thus be described by the following general equations:

$$\frac{d\phi}{dt} = K_{1i0}(P) \cdot exp\left[\frac{-H(P)}{T}\right] \cdot \frac{(1-\phi)^k}{\eta^m} \quad (14)$$

$$\frac{d\eta}{dt} = K_{2i0}(P) \cdot exp\left[\frac{-L(P)}{T}\right] \cdot \frac{1}{(1-\phi)^\ell \cdot \eta^{n-1}} \quad (15)$$

which may be expected to satisfactorily reproduce the experimental data (development of ϕ and η with time, for any test sintering temperature and green microstructure).

This analytical method allows refinement of parameters K_{1i} and K_{2i}, estimated by the differential method, yielding more accurate values[36].

To obtain highly densified bulk samples, the sintering stage must be conducted at the maximum allowable sintering temperature (according to equation 14). However, high sintering temperatures also result in high grain growth rates (equation 15), which could lead to abnormal grain growth. It is therefore not advisable to select an extremely high, constant sintering temperature because heterogeneous (or even extremely coarse-grained) sintered microstructures could be obtained, worsening the final properties of the polycrystalline bulk material[7,37,38]. In addition, the grain growth rate is usually higher than the densification rate, adding a further challenge to thermal cycle design.

3.4. Using densification and grain growth rate equations to design an optimal thermal sintering cycle

In light of the above, thermal cycle design needs to observe the following general guidelines: (i) Sintering shall take place at the maximum allowable temperature for a particular dwell time ($t_{dwell,T}$), defined by the constraint that no exaggerated grain growth

take place. (ii) After this dwell time has elapsed, sintering temperature shall be lowered and kept constant again for a further period of time, defined by the same constraint. Lowering sintering temperature decreases both densification and grain growth rates, while allowing the densification process to be kept at the highest possible values, controlling grain growth and preventing abnormal grain growth[39,40]. (iii) This gradual decrease in sintering temperature may be carried out as often as required, provided acceptable values are obtained for the densification rate.

To determine the dwell time at each sintering temperature, the following method shall be followed: (i) simultaneous numerical integration of the densification and grain growth rate equations (eq. 14 and 15) at the set temperature, yielding the development of ϕ and η with time (t); (ii) substitution of the t, ϕ, and η values in equations 14 and 15 in order to determine the densification rate and the grain growth rate ($d\phi/dt$ and $d\eta/dt$) with sintering time (t) (Figure 9); and (iii) determination of the vertex of each rate curve in Figure 5, calculated as the intersection of the tangents to the two branches of the rate curves (corresponding to zero and infinite sintering times).

As may be observed in Figure 9, two dwell times are obtained: one for the densification rate curve (t_d) and the other for the grain growth rate curve (t_g). The shorter time shall be chosen as the dwell time at the set temperature ($t_{dwell,T}$). This value is selected for $t_{dwell,T}$ because: (i) it corresponds to the dwell time at which the densification and grain growth rates stop dropping sharply and start to decrease more slowly, an effect that is usually more pronounced at higher sintering temperatures; and (ii) at longer times, the differences between the densification rate and the grain growth rate values are greater (distance between the curves).

Figure 10 compares a staggered thermal cycle, designed by the above method, with a single step-up thermal cycle. The grain growth and densification rates are plotted against sintering time for the two (staggered and single step-up) thermal cycles in Figure 11. The gradual decrease in maximum sintering temperature is observed to significantly reduce the grain growth rate, while hardly changing the densification rate. This may be expected to allow densification of the polycrystalline solid material to a relative density close to its theoretical value, while providing precise control of grain growth. The figure also shows that the grain growth rate is always higher than the densification rate, which is the worst, albeit most common, scenario in solid-state sintering of polycrystalline ceramic materials.

The staggered thermal cycle shown in Figure 10 allows sintered bulk materials with high relative density (close to theoretical density) and fine, narrow, homogeneous grain size distribution to be obtained, thus assuring the targeted final properties of the materials for their specific application. In addition, such staggered thermal cycles may provide an important reduction in sintering stage duration, compared with that of the traditional single step-up thermal cycle.

The steps of the proposed staggered thermal cycle could be replaced with an empirical continuous mathematical function (polynomial function of time including power and exponential terms), representing the gradual decrease in sintering temperature with sintering time.

4. CONCLUSIONS

1. A new method has been developed to determine the optimal sintering conditions for obtaining bulk polycrystalline solids with the appropriate microstructure for targeted product performance. This method is valid for final-stage solid-state sintering, which is the critical stage in the manufacturing of near fully dense

sintered bodies, since the first sintering stages are negligible because of the high density of the initial green bodies.

2. The theoretical bases of this method are reported in the literature and have been reviewed in this paper.
3. Studies in the literature have modelled simple particulate systems, but the proposed method can be applied to real particulate solids with high final density.
4. The method allows a staggered thermal sintering cycle (number of steps, sintering temperature, and dwell time) to be set, based on promoting the densification rate over the grain growth rate, keeping in mind the main microstructural control parameters, average grain size, and relative density in order to achieve the targeted performance of the final bulk ceramic.
5. In addition, the method also enables the mass transfer-controlling mechanisms occurring in densification and grain growth to be determined.
6. The method has been successfully tested and validated for nickel–zinc micro-ferrite ceramics, after designing the manufacturing thermal sintering cycle and obtaining the mass transport-controlling mechanisms for densification (grain boundary diffusion) and grain growth (surface diffusion pore-drag control).

ACKNOWLEDGEMENTS

This study has been funded by the Spanish National Plan for Scientific Research, Development, and Technology Innovation of the Spanish Ministry of Economy and Competitiveness (project MAT2016-76320-R) and Jaume I University of Spain (project UJI-B2017-48).

NOMENCLATURE

γ: surface energy (J/m^2)

γ_{s-g}: solid–gas surface energy (J/m^2)

γ_{s-s}: solid–solid surface energy (J/m^2)

Γ: ratio of grain growth rate to densification rate

η: dimensionless grain size

ρ: body density (kg/m^3)

ρ_t: theoretical density (kg/m^3)

ϕ: relative density

Ω: volume of material moved in association with one ion of the rate-controlling species (m^3/mol)

C_d: constant related to the densification-controlling mechanism

C_g: constant related to the grain growth-controlling mechanism

d_{50}: average particle size in the green body (μm)

A: surface area (m^2)

H: pre-exponential factor in equation 7, according to the Arrhenius law (K)

L: pre-exponential factor in equation 8, according to the Arrhenius law (K)

D_d: diffusion coefficient of the densification process (cm^2/s)

D_g: diffusion coefficient of the grain growth process (cm^2/s)

F_a: force acting on the atoms (N)

F_{gb}: force acting on the grain boundary (N)

F_p: force acting on the pore (N)

G: average grain size in the sintered body (μm)

J_{1i}: proportional constant in equation 1

J_{2i}: proportional constant in equation 2

K: Boltzmann constant (J/K)

k: coefficient in equation 1, dependent on the densification mass transfer mechanism

K_{1i}: proportional constant in equation 5 (s^{-1})

K_{1i0}: exponential factor in equation 7, according to the Arrhenius law (s^{-1})

K_{2i}: proportional constant in equation 6 (s^{-1})

K_{2i0}: exponential factor in equation 8, according to the Arrhenius law (s^{-1})

ℓ: coefficient in equation 2, dependent on the grain growth mass transfer mechanism

m: coefficient in equation 1, dependent on the densification mass transfer mechanism

M_a: atomic mobility (m/N·s)

M_{gb}: grain boundary mobility (m/N·s)

M_p: pore mobility (m/N·s)

M_s: grain boundary mobility only due to the solute atom concentration gradient (m/N·s)

M_0: original grain boundary mobility, without dopants (m/N·s)

n: coefficient in equation 2, dependent on the grain growth mass transfer mechanism

N: number of pores per grain

P: selected shaping parameter (e.g. pressing pressure)

T: sintering temperature (K)

t: sintering time (h)

t_d: dwell time determined for the densification rate curve

t_g: dwell time determined for the grain growth rate curve

$t_{dwell,T}$: dwell time at a given temperature in the thermal cycle design

v_a: atomic migration rate (m/s)

v_{gb}: grain boundary migration rate (m/s)

v_p: pore migration rate (m/s)

REFERENCES

[1] M.N. Rahaman, Ceramic Processing, CRC Press, Boca Ratón, Florida, 2007.

[2] M.N. Rahaman, Ceramic processing and sintering, Second Edi, Marcel Dekker, Inc, New York, 2003.

[3] S.L. Kang, Sintering Densification,Grain Growth,and Microstructure, Elsevier Butterworth-Heinemann, Oxford, 2005. doi:http://dx.doi.org/10.1016/B978-075066385-4/50009-1.

[4] F. Li, J. Pan, Modelling '"Nano-Effects"' in Sintering, in: R. Castro, K. van Benthem (Eds.), Sintering, Springer, 2013: pp. 17–34. doi:10.1007/978-3-642-31009-6.

[5] S.J.L. Kang, Y. Il Jung, Sintering kinetics at final stage sintering: Model calculation and map construction, Acta Mater. 52 (2004) 4573–4578. doi:10.1016/j.actamat.2004.06.015.

[6] M.F. Yan, R.M. Cannon, H.K. Bowen, U. Chowdhry, Effect of grain size distribution on sintered density, Mater. Sci. Eng. 60 (1983) 275–281. doi:10.4028/www.scientific.net/MSF.94-96.331.

[7] M.F. Yan, Microstructural control in the processing of electronic ceramics, Mater. Sci. Eng. 48 (1981) 53–72. doi:10.1016/0025-5416(81)90066-5.

[8] F. Wakai, Modeling and simulation of elementary processes in ideal sintering, J. Am. Ceram. Soc. 89 (2006) 1471–1484. doi:10.1111/j.1551-2916.2006.01001.x.

[9] G.N. Hassold, I. -W Chen, D.J. Srolovitz, Computer Simulation of Final-Stage Sintering: I, Model Kinetics, and Microstructure, J. Am. Ceram. Soc. (1990). doi:10.1111/j.1151-2916.1990.tb06686.x.

[10] I. -W Chen, G.N. Hassold, D.J. Srolovitz, Computer Simulation of Final-Stage Sintering: II, Influence of Initial Pore Size, J. Am. Ceram. Soc. (1990). doi:10.1111/j.1151-2916.1990.tb06687.x.

[11] A. Maximenko, A. Kuzmov, E. Grigoryev, E. Olevsky, Direct multi-scale modeling of sintering, J. Am. Ceram. Soc. 95 (2012) 2383–2388. doi:10.1111/j.1551-2916.2012.05083.x.

[12] Z.Z. Fang, H. Wang, Densification and grain growth during sintering of nanosized particles, Int. Mater. Rev. 53 (2008) 326–352. doi:10.1179/174328008X353538.

[13] K. Abdelrazek, Advanced Sintering of Nano-Ceramic Materials, in: Prof. Feng Shi (Ed.), Ceram. Mater. - Prog. Mod. Ceram., InTech, Shanghai, China, 2012: pp. 65–82. doi:10.5772/38287.

[14] K. Lu, Sintering of nanoceramics, Int. Mater. Rev. 53 (2008) 21–38. doi:10.1179/174328008X254358.

[15] R. Chaim, M. Levin, A. Shlayer, C. Estournes, Sintering and densification of nanocrystalline ceramic oxide powders: a review, Adv. Appl. Ceram. 107 (2008) 159–169. doi:10.1179/174367508X297812.

[16] A. Barba, C. Clausell, C. Felíu, M. Monzó, Sintering of (Cu0.25Ni0.25Zn0.50)Fe2O4Ferrite, J. Am. Ceram. Soc. 77 (2004) 571–577.

[17] C. Clausell, A. Barba, Processing-microstructure-properties relationship in a CuNiZn ferrite, Bol. Soc. Esp. Ceram. Vidr. (2017). doi:10.1016/j.bsecv.2017.09.002.

[18] A. Barba, C. Clausell, M. Monzó, J.C. Jarque, M. Monzó, J.C. Jarque, Thermal cycle for obtaining a Ni-Zn ferrite: (I) Design of the sintering stage, Boletín La

Soc. Española Cerámica y Vidr. 47 (2008) 13–23. doi:10.3989 / cyv.2004.v43.i5.

[19] N.J. Shaw, Densification and coarsening during solid state sintering of ceramics: a review of the models. I Densification, Powder Metall. Int. 21 (1989) 17–21.

[20] N.J. Shaw, Densification and coarsening during solid state sintering of ceramics: a review of the models. II Grain growth, Powder Metall. Int. 21 (1989) 31–33.

[21] N.J. Shaw, Densification and coarsening during solid state sintering of ceramics: a review of the models. III Coarsening, Powder Metall. Int. 21 (1989) 25–29.

[22] B.J. Kellett, F.F. Lange, Thermodynamics of Densification: I, Sintering of Simple Particle Arrays, Equilibrium Configurations, Pore Stability, and Shrinkage, J. Am. Ceram. Soc. 72 (1989) 725–734. doi:10.1111/j.1151-2916.1989.tb06208.x.

[23] F.F. Lange, B.J. Kellett*, Thermodynamics of Densification: II, Grain Growth in Porous Compacts and Relation to Densification, J. Am. Ceram. Soc. 72 (1989) 735–741. doi:10.1111/j.1151-2916.1989.tb06209.x.

[24] J.L. Shi, Thermodynamics and densification kinetics in solid-state sintering of ceramics, J. Mater. Res. (1999). doi:10.1557/JMR.1999.0190.

[25] R.L. Coble, Sintering Crystalline Solids. I, Intermediate and Final State Diffusion Models, Appl. Phys. (1961). doi:doi:10.1063/1.1736107.

[26] B.M. Smirnov, Chapter 14. General Principles of Transport Phenomena, in: Princ. Stat. Phys. Distrib. Struct. Phenomena, Kinet. At. Syst., Wiley-VCH Verlag GmbH & Co. KGaA, 2006: pp. 249–269.

[27] R.J. Brook, Pore-Grain Boundary Interactions and Grain Growth, J. Am. Ceram. Soc. 52 (1969) 56–57.

[28] J. Zhao, M.P. Harmer, Effect of Pore Distribution on Microstructure Development: I, Matrix Pores, J. Am. Ceram. Soc. 71 (1988) 113–120. doi:10.1111/j.1151-2916.1988.tb05826.x.

[29] J. Zhao, M.P. Harmer, Effect of Pore Distribution on Microstructure Development: II, First- and Second-Generation Pores, J. Am. Ceram. Soc. 71 (1988) 530–539. doi:10.1111/j.1151-2916.1988.tb05916.x.

[30] J. Zhao, M.P. Harmer, Effect of Pore Distribution on Microstructure Development: III, Model Experiments, J. Am. Ceram. Soc. 75 (1992) 830–843. doi:10.1111/j.1151-2916.1992.tb04148.x.

[31] H. Hsueh, A.G. Evans, R.L. Coble, Microstructure development during final/intermediate stage sintering, Acta Materalia. (1982).

[32] H. Su, D.L. Johnson, Master Sintering Curve: A Practical Approach to Sintering, J. Am. Ceram. Soc. 79 (1996) 3211–3217. doi:10.1111/j.1151-2916.1996.tb08097.x.

[33] J.D. Hansen, R.P. Rusin, M.-H. Teng, D.L. Johnson, Combined-Stage Sintering Model, J. Am. Ceram. Soc. 75 (1992) 1129–1135. doi:10.1111/j.1151-2916.1992.tb05549.x.

[34] Z.Z. Du, A.C.F. Cocks, Constitutive models for the sintering of ceramic components-I. Material models, Acta Metall. Mater. (1992). doi:10.1016/0956-7151(92)90183-F.

[35] R. Vasudevan, T. Karthik, S. Ganesan, R. Jayavel, Effect of microwave sintering on the structural and densification behavior of sol–gel derived zirconia toughened alumina (ZTA) nanocomposites, Ceram. Int. 39 (2013) 3195–3204.

doi:10.1016/j.ceramint.2012.10.004.

[36] O. Levenspiel, Chemical Reaction Engineering, Third Edit, John Wiley & Sons, Inc., New York, 1999. doi:10.1021/ie990488g.

[37] A.M. Glaeser, Investigating surface transport in ceramics using microdesigned interfaces, in: R. Smart, J. Nowotny (Eds.), Ceram. Interfaces Prop. Appl., IOM Communications, London, 1998: pp. 241–282.

[38] R.J. Brook, Fabrication principles for the production of ceramics with superior mechanical properties, in: R.W. Davidge (Ed.), Eng. with Ceram. Proc. Br. Ceram. Soc., Vol.32, British Ceramic Society, Stoke-on-Trent, UK, 1982: pp. 7–24.

[39] X.H. Wang, P.L. Chen, I.W. Chen, Two-step sintering of ceramics with constant grain-size, I. Y 2O 3, J. Am. Ceram. Soc. 89 (2006) 431–437. doi:10.1111/j.1551-2916.2005.00763.x.

[40] H. Su, X. Tang, H. Zhang, Z. Zhong, J. Shen, Sintering dense NiZn ferrite by two-step sintering process, J. Appl. Phys. 109 (2011) 83–85. doi:10.1063/1.3535418.

FIGURE CAPTIONS

FIGURE 1 Driving forces for solid-state sintering processes

FIGURE 2 The Brook model: grain size versus pore size

FIGURE 3 General development of dimensionless grain size ($\boldsymbol{\eta}$) with relative density ($\boldsymbol{\phi}$) at different sintering temperatures (T). (Graph valid for given shaping conditions): equations 10 and 11

FIGURE 4 Overview of a general method for simultaneous determination of densification and grain growth in final-stage solid-state sintering in order to define optimal thermal cycles

FIGURE 5 General development of dimensionless densification ($\boldsymbol{\phi}$) with sintering time ($\boldsymbol{t}$) at different sintering temperatures ($\boldsymbol{T}$). (Graph valid for given shaping conditions)

FIGURE 6 General development of dimensionless grain size ($\boldsymbol{\eta}$) with sintering time ($\boldsymbol{t}$) at different sintering temperatures ($\boldsymbol{T}$). (Graph valid for given shaping conditions)

FIGURE 7 $\boldsymbol{ln(d\phi/dt) - k \cdot ln(1-\phi)}$ as a function of $\boldsymbol{ln(\eta)}$ for the $\boldsymbol{K_{1i}}$ and $\boldsymbol{m}$ values obtained, for a given $\boldsymbol{k}$ value

FIGURE 8 $\boldsymbol{ln(d\eta/dt) + \ell \cdot ln(1-\phi)}$ as a function of $\boldsymbol{ln(\eta)}$ for the $\boldsymbol{K_{2i}}$ and $\boldsymbol{(n-1)}$ values obtained, for a given $\boldsymbol{\ell}$ value

FIGURE 9 Methodology for determining the maximum dwell time ($\boldsymbol{t_d/t_g}$) at a given sintering temperature ($\boldsymbol{t_{dwell,T}}$)

FIGURE 10 Single step-up vs staggered thermal cycle for the sintering stage

FIGURE 11 Comparison of the densification and grain growth rates of a single step-up and a staggered thermal cycle

TABLES

TABLE 1 Mass transfer-controlling mechanisms in densification and corresponding values of the k and m coefficients in equation 5

Diffusion path	i	k	m
Volume or bulk diffusion	1	1/3	3
Grain boundary diffusion	2	0	4

TABLE 2 Conditions of grain boundary migration and mass transfer-controlling mechanisms in grain growth and corresponding values of the ℓ and n coefficients in equation 6

Grain boundary migration	Mass transfer mechanism	i	ℓ	n
Pore control	Surface diffusion	1	4/3	4
	Volume diffusion	2	1	3
	Gas phase diffusion	3	1	3
	Evaporation–Condensation	4	2/3	2
Boundary control	Grain boundary diffusion	5	0	2

Figure

Click here to download high resolution image

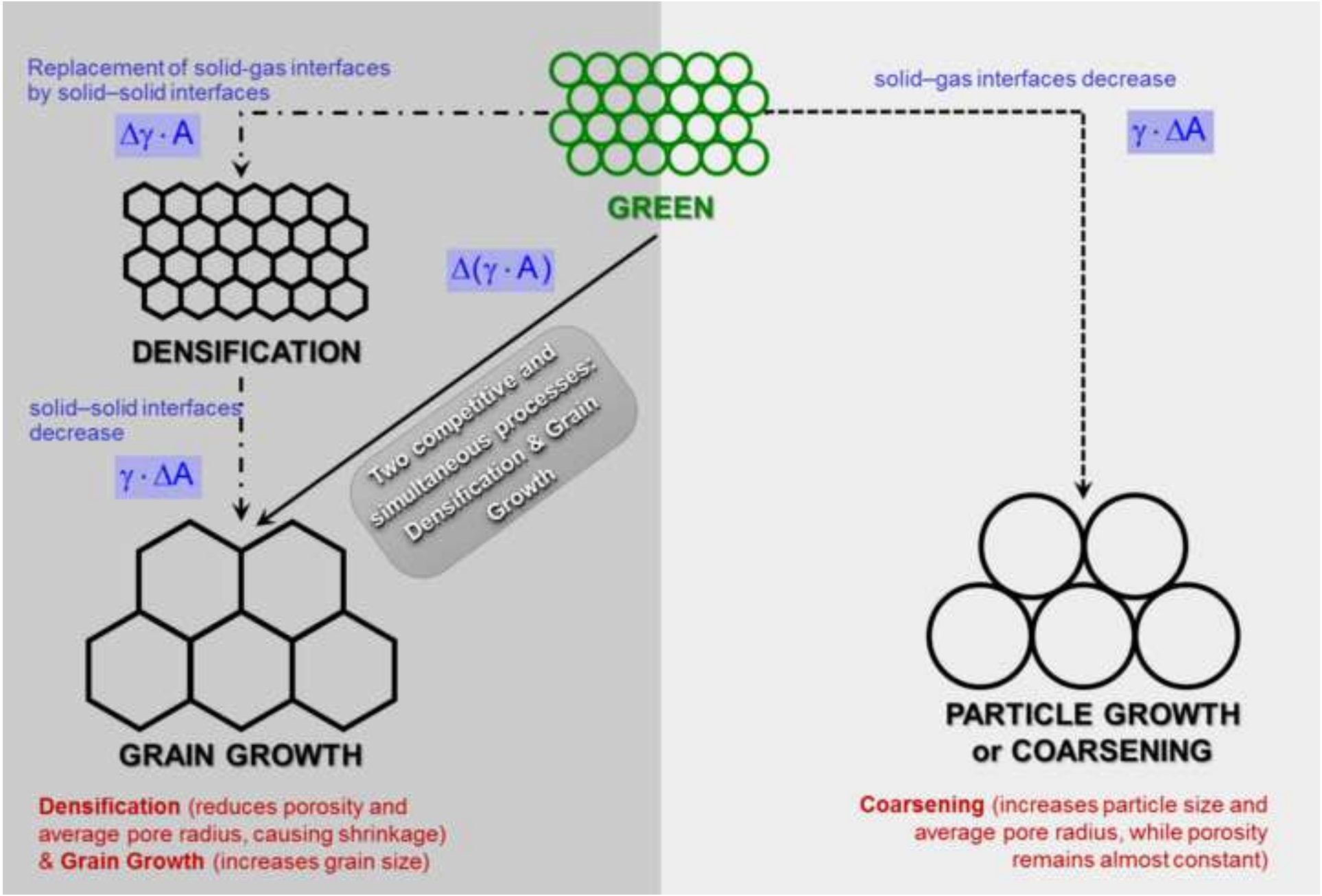

Figure
Click here to download high resolution image

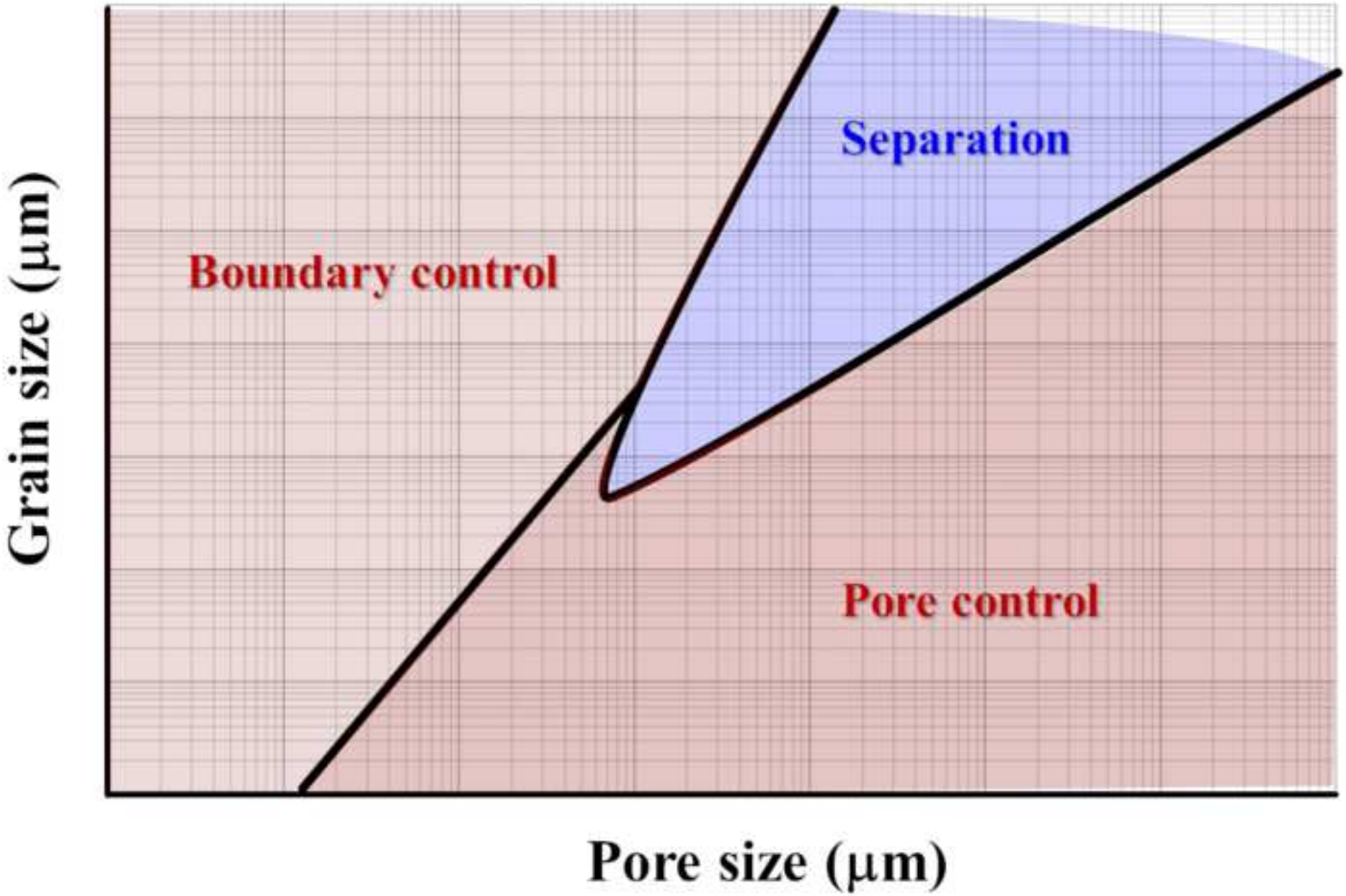

Figure

Click here to download high resolution image

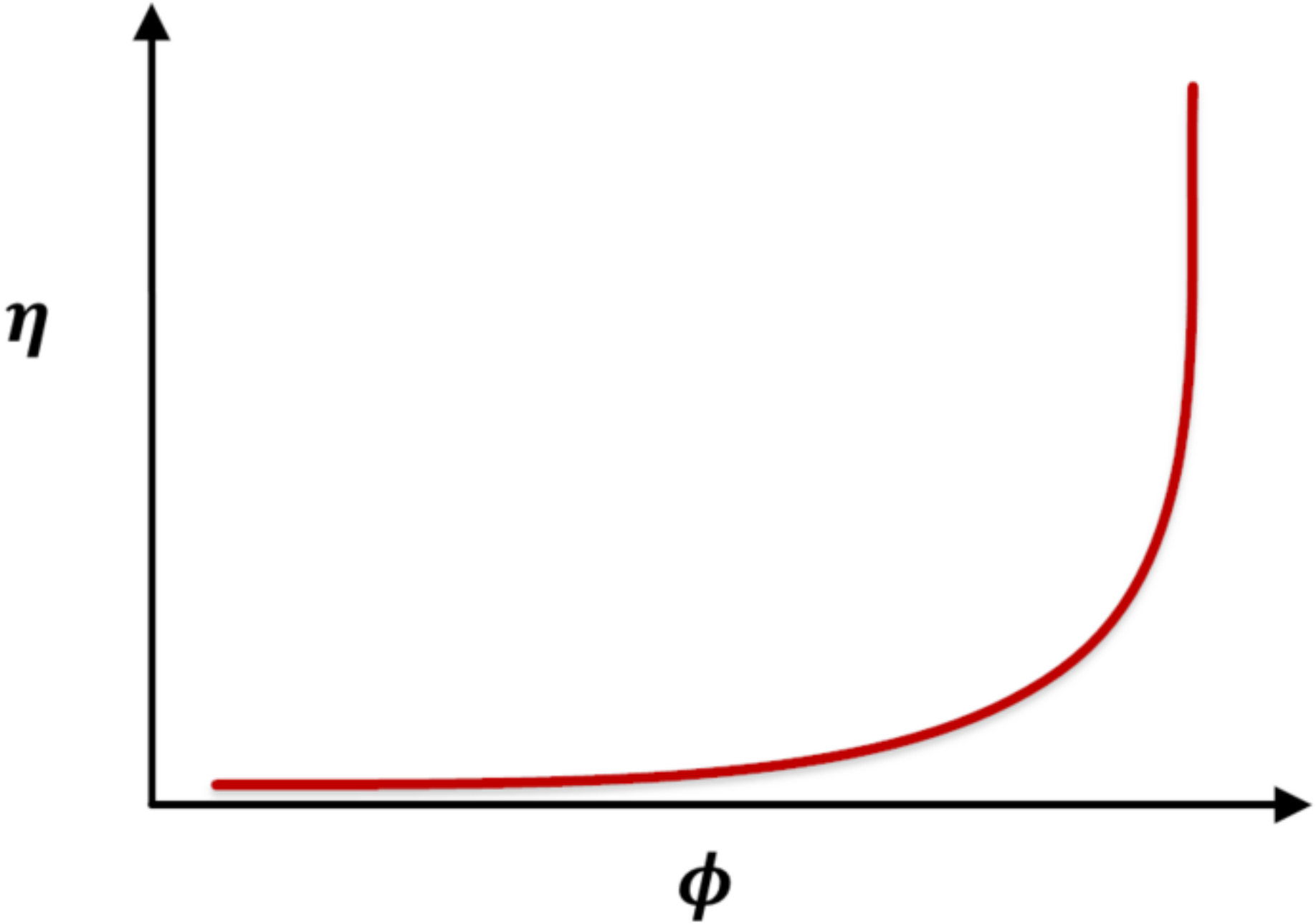

Figure
Click here to download high resolution image

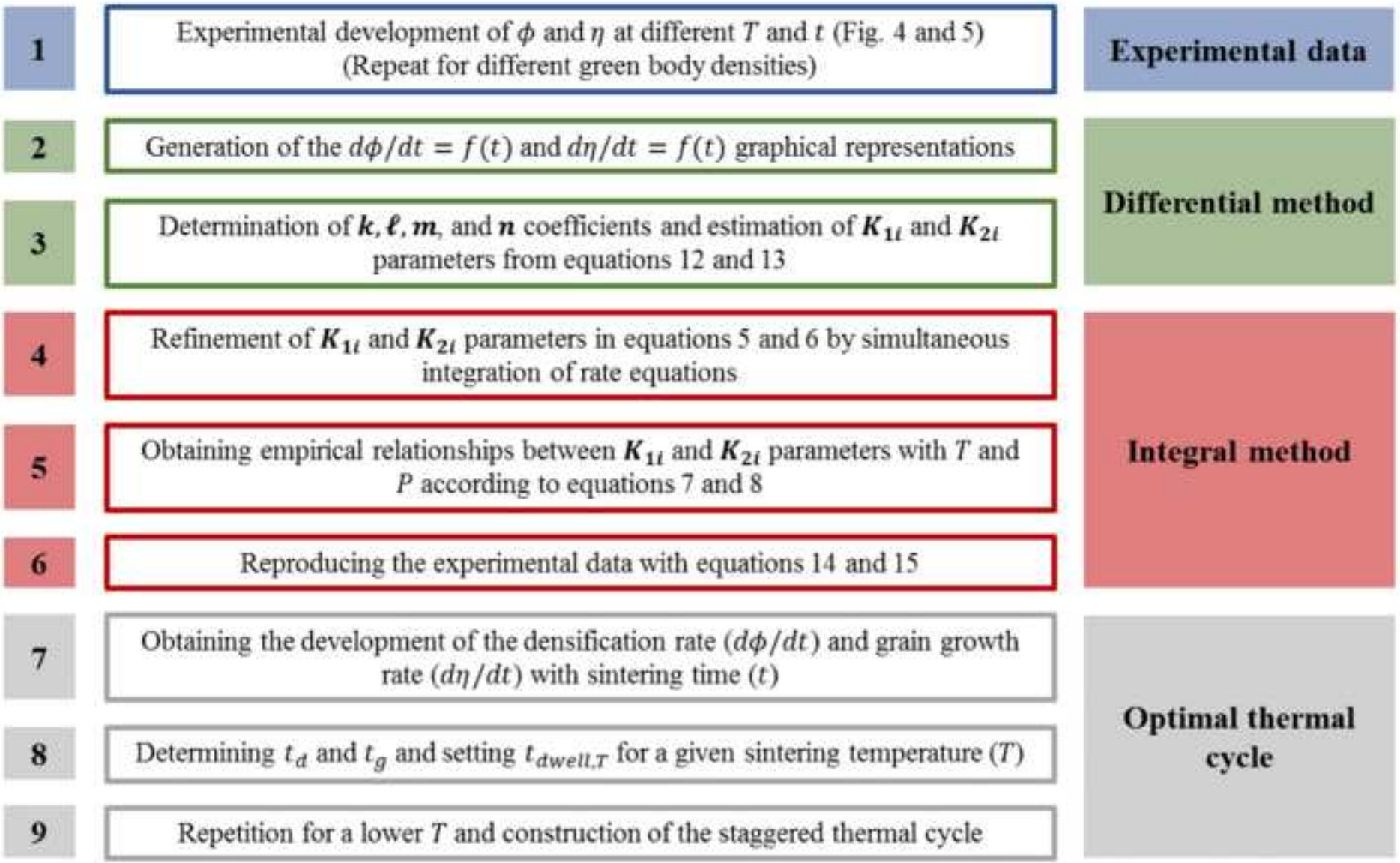

Figure

Click here to download high resolution image

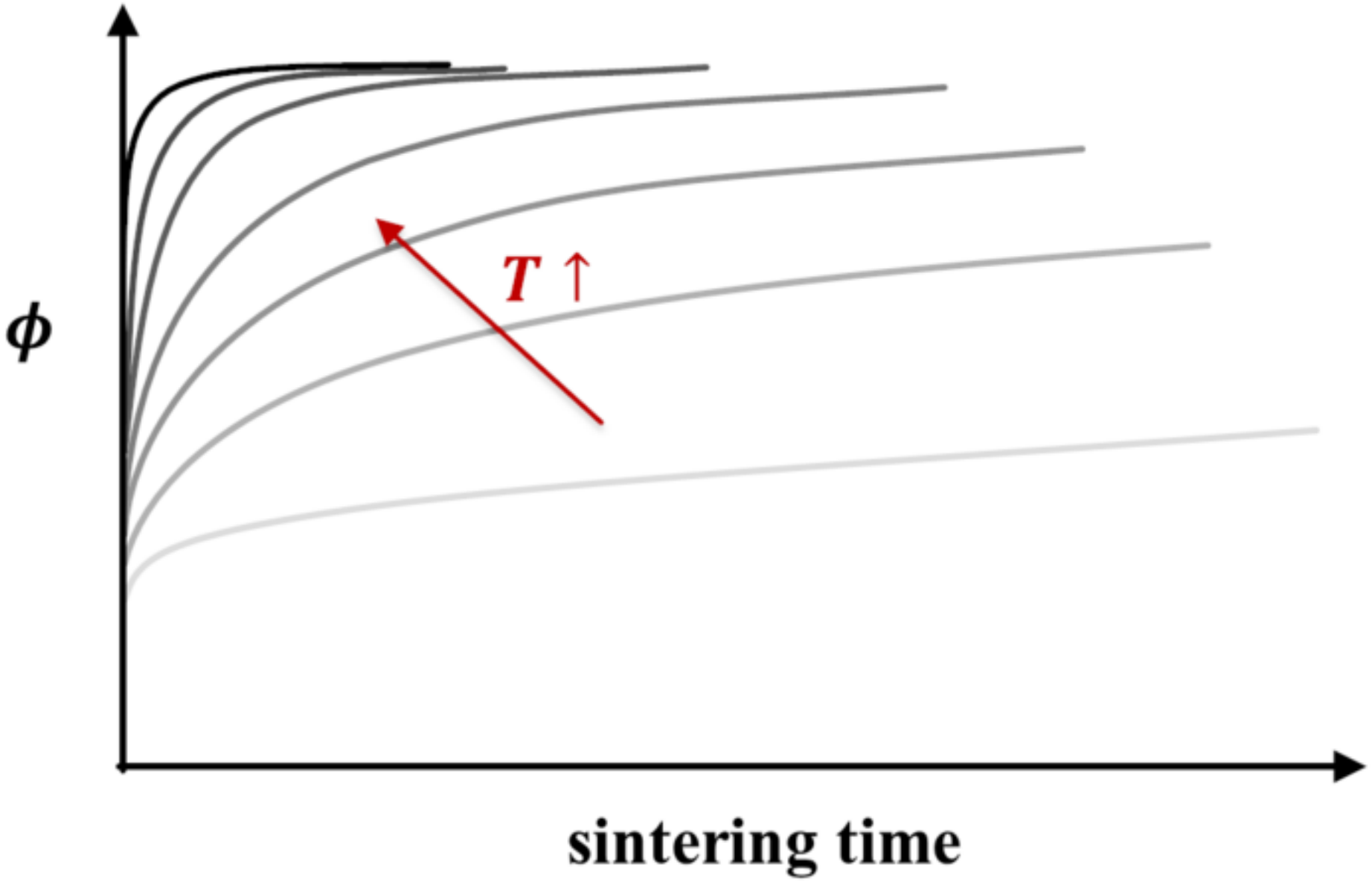

Figure

Click here to download high resolution image

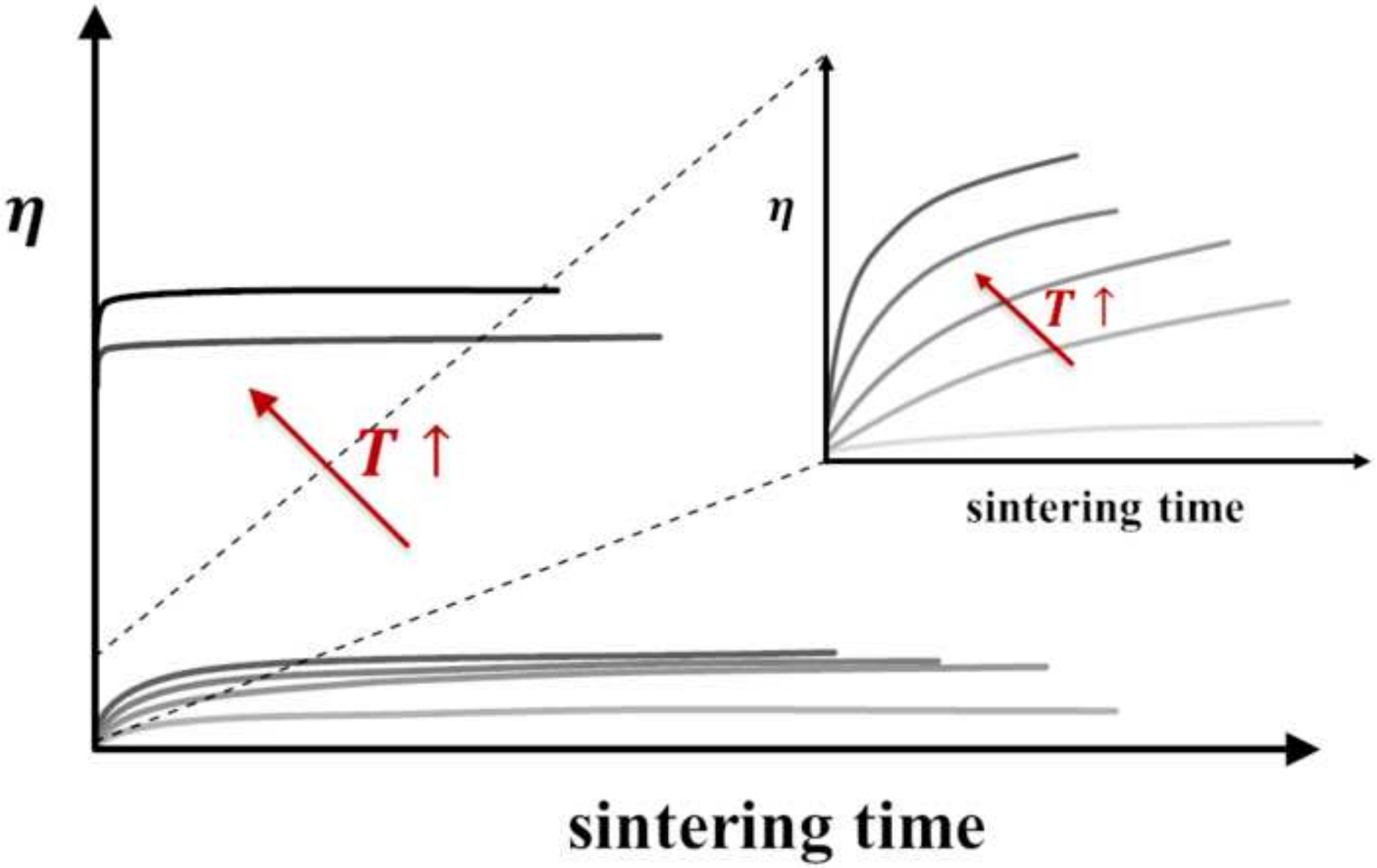

Figure

Click here to download high resolution image

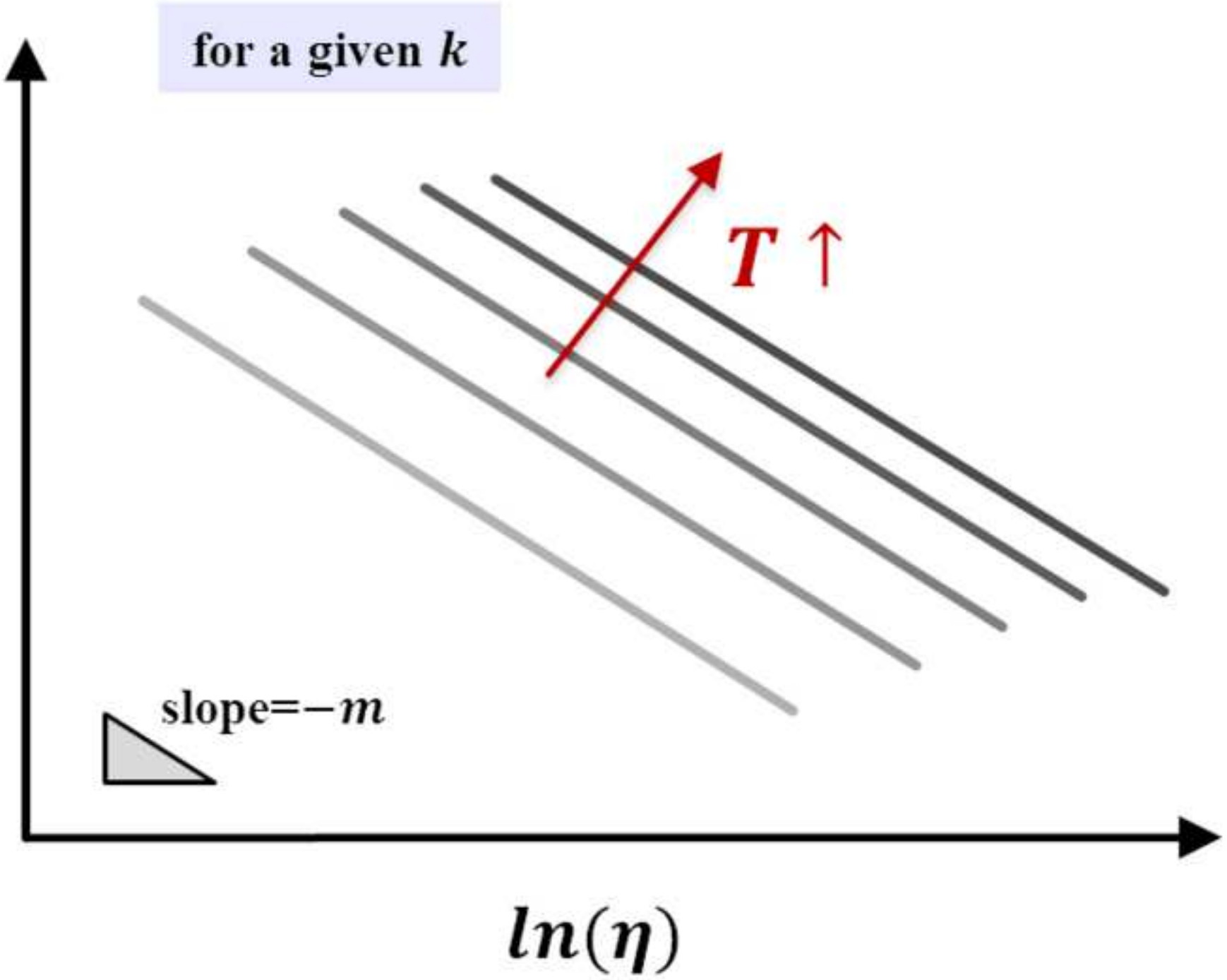

Figure

Click here to download high resolution image

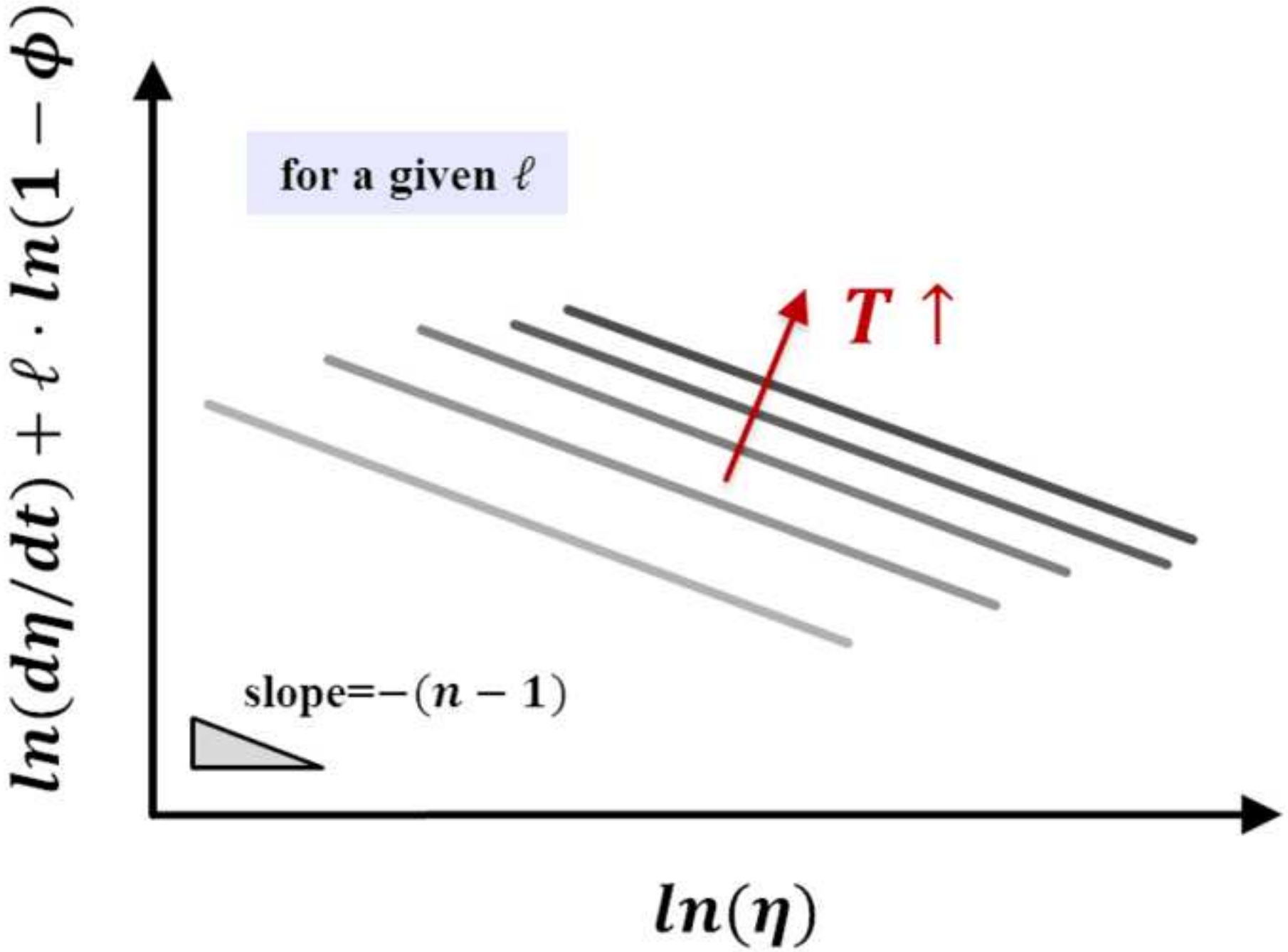

Figure
Click here to download high resolution image

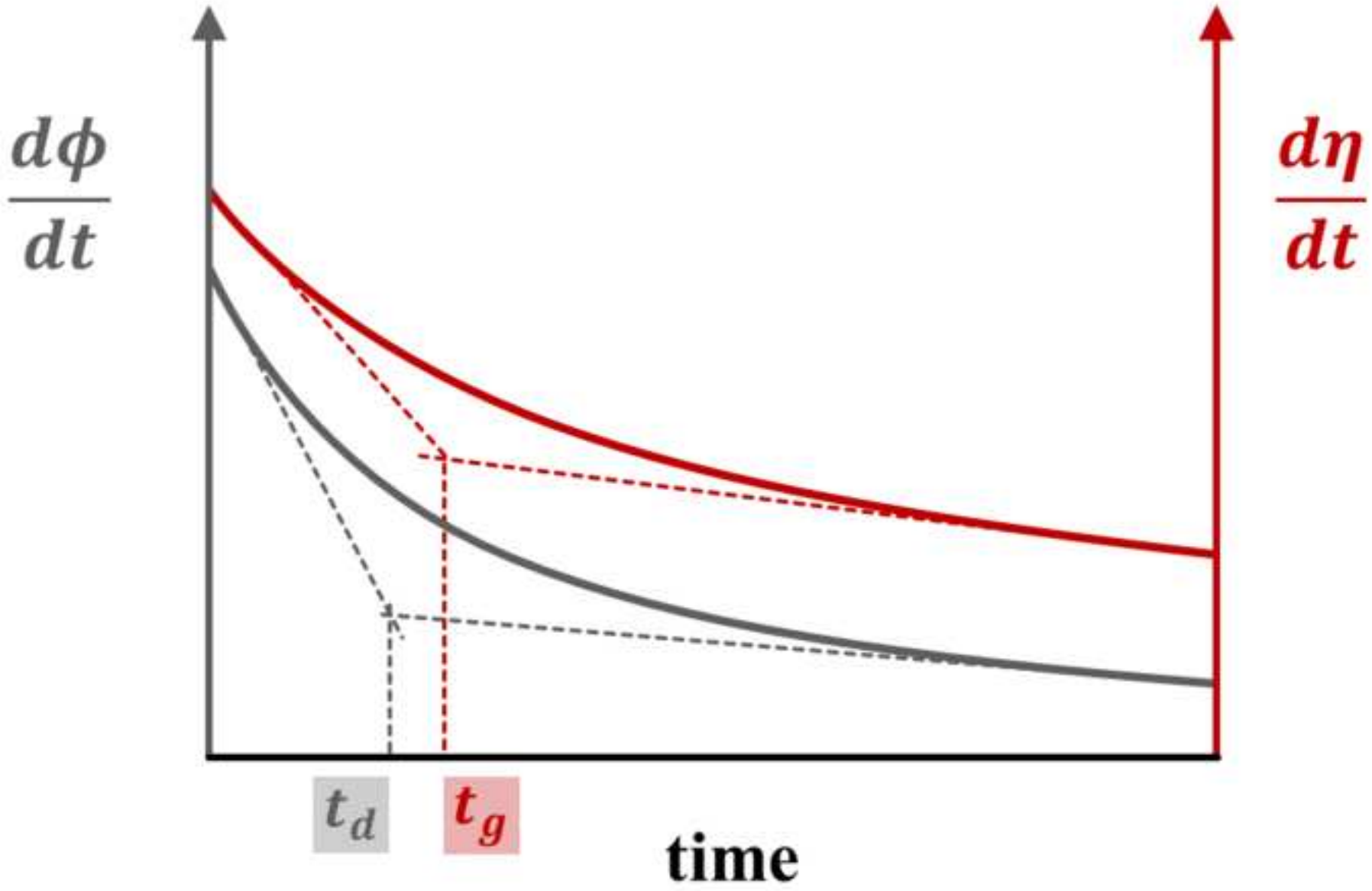

Figure
Click here to download high resolution image

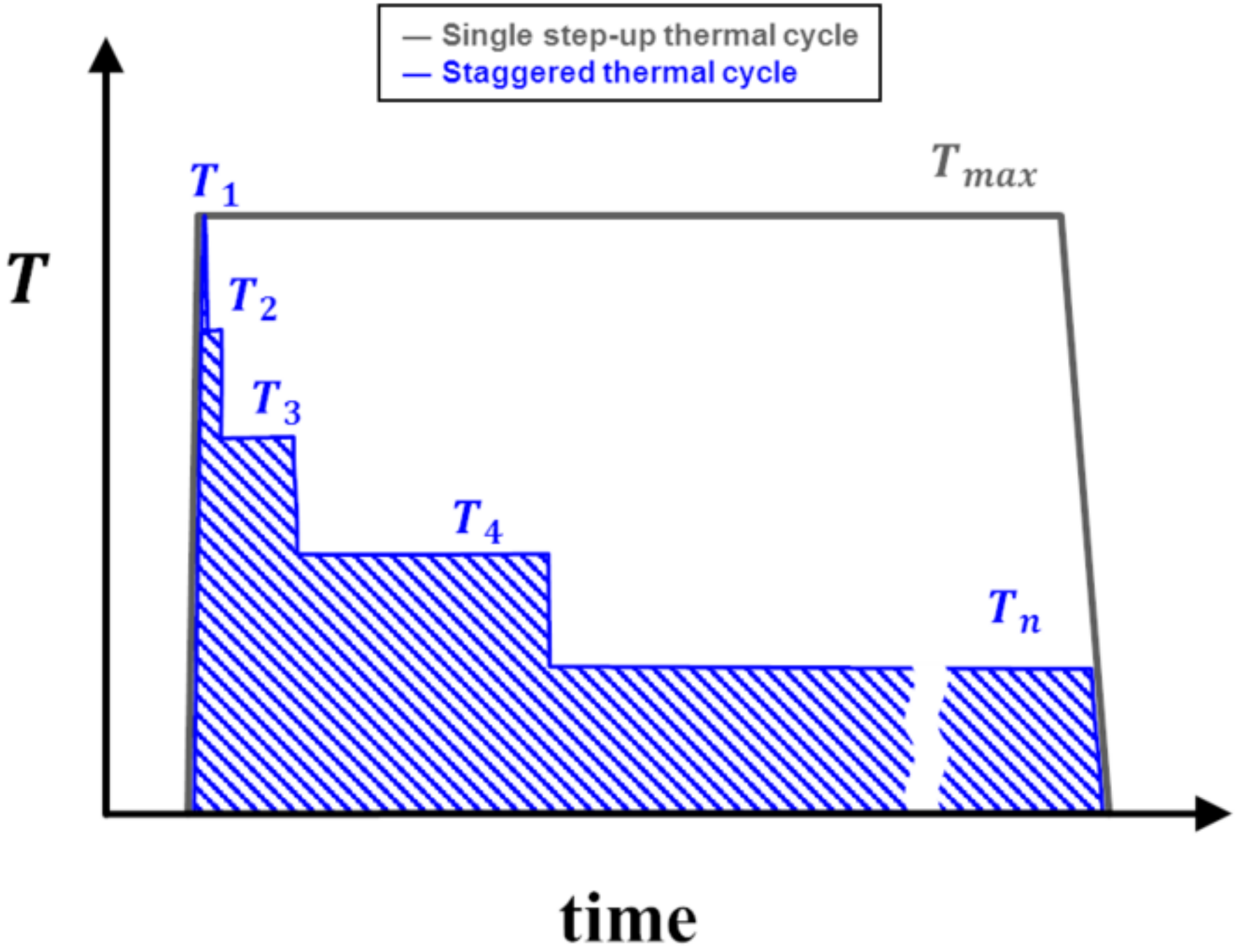

Figure
Click here to download high resolution image